Coding Metasurface for Talbot Sound Amplification

He Gao,[1,‡] Zhongming Gu,[1,2,‡] Shanjun Liang,[1,3] Shuowei An,[1] Tuo Liu,[1,2,*] and Jie Zhu[1,2,4,†]

[1] *Department of Mechanical Engineering, The Hong Kong Polytechnic University, Hung Hom, Kowloon, Hong Kong SAR, China*

[2] *The Hong Kong Polytechnic University Shenzhen Research Institute, Shenzhen 518057, People's Republic of China*

[3] *Division of Science, Engineering and Health Studies, College of Professional and Continuing Education, Hong Kong Polytechnic University, Kowloon, Hong Kong SAR, China*

[4] *Research Center for Fluid-Structure Interactions, Hong Kong Polytechnic University, Kowloon, Hong Kong SAR, China*

(Received 7 August 2020; revised 1 November 2020; accepted 3 November 2020; published 25 November 2020)

The Talbot effect has found profound applications in a wide variety of research fields, facilitating the development of sensing, imaging, and lithography, among others. Taking advantage of the flexibilities offered by the bidimensional Talbot effect, we propose and experimentally demonstrate a 2-bit coding acoustic metasurface lens. It is capable of arranging the far-field wave-energy distribution and thus tailoring the passive amplification of wave pattern at positions away from the source. By simply adjusting two different types of embedded helicoid units and their layout in the metasurface lens to change the coding sequences, the intensity amplification factor and period of the self-image can be manipulated simultaneously within the same imaging plane. The proposed Talbot lens allows flexible far-field sound redistribution and enhancement. Along with the nonresonant nature, it may open possibilities in applications such as acoustic communication, sonography, and signal processing.

DOI: 10.1103/PhysRevApplied.14.054067

I. INTRODUCTION

Passively enhancing acoustic field and wave pattern can intensify sound signals as well as strengthen the wave-matter interaction effects without introducing the complex setup of active sources. It benefits numerous applications in acoustic sensing [1], sound detection [2], and biomedical imaging [3], etc. The recent development of acoustic metamaterials has inspired several innovative approaches towards different enhancement effects [4–16]. Space-coiled cavities operating at resonance are able to localize the sound energy in the deep-subwavelength scale [4,5], yet suffer from narrow bandwidth. To lift this restriction, the so-called rainbow-trapping design [6–9] was proposed, in which broadband acoustic waves are decelerated and compressed to create spatial-spectral concentrations of sound energy. But still, the resonance-based building blocks are highly dispersive in nature and remain sensitive to the thermal and viscous losses [6,12]. An alternative approach utilizes high impedance metafluid together with an impedance-matched layer to present a feasible way of boosting acoustic pressure over the spectrum [13,14]. However, for the mentioned strategies, they are only suitable for the near field where the enhanced sound field is confined within the metamaterials, resultantly limiting the application potentials. How to achieve remote sound-field and wave-pattern enhancement in a passive way with nonresonant structures, extremely valuable in applications as it would be, remains an unsolved challenge.

The Talbot effect, also known as self-imaging, is capable of passively repeating incident wave pattern. It was discovered and explained in the context of classical wave-diffraction physics [17,18]. Rayleigh gave an explanation of the Talbot effect as a result of the interference between the diffraction orders and showed that any periodic one-dimensional field pattern reappeared at integer multiples of the so-called Talbot length [18]. In addition to the integer Talbot effect, fractional self-images are formed at propagation distances that are equal to a fraction of Talbot length [19,20]. The simplicity and diversity of this effect have since beautifully triggered a wave of research across different frontier disciplines [17–29], facilitating the development of wave-front sensing [24], lithography [25], and optical waveform amplification [23], etc. The recent combination of optical self-imaging with phase-manipulation

*tuoliu@polyu.edu.hk
†jiezhu@polyu.edu.hk
‡These authors contributed equally to this work.

technology even offers great flexibilities associated with the Talbot effect and multifunctionalities [21].

In this work, we demonstrate the bidimensional Talbot effect and its unique far-field sound-pattern manipulation capability. By incorporating the integer Talbot self-imaging [18] and fractional Talbot self-imaging [19], we present a passive acoustic Talbot amplifier that is able to not only redistribute the wave pattern but also enhance the field signal remotely. Such far-field Talbot amplification is practically realized with a 2-bit isotropic coding metasurface whose discrete elements, each containing one of the four digital states (phase delay) "00" (0), "01"($\pi/2$), "10" (π), and "11" ($3\pi/2$), are implemented using helicoid metamaterials [11]. These four digital elements can be arranged in different coding sequences to create various Talbot self-imaging patterns. Such digital discretization of phase profiles can substantially reduce the parameter search space during the design optimization and simplify the device design procedure [30–34]. Our study indicates an efficient approach to passively achieve the far-field enhancement of sound pattern in free space, as well as a promising direction to exploit the Talbot effect and its application potential in acoustic systems.

II. DESIGN PRINCIPLE OF THE CODING METASURFACE

The proposed coding metasurface is composed of unit cells periodically distributed within a two-dimensional space, as illustrated in Fig. 1. The unit cell has four elements arranged in a 2×2 fashion. Each element, by design, can realize one of the 0, $\pi/2$, π, and $3\pi/2$ phase delays to the incident wave, respectively, corresponding to "00", "01", "10", and "11" in the 2-bit 4-digital states. When an incoming sound pattern illuminates the designed coding metasurface, applying different spatial-coding arrangements can realize various distinctive images at the same diffraction distance [21].

The design principle of realizing Talbot sound amplification is shown in Fig. 2. For an acoustic Talbot-coding metasurface without any phase modulation, all unit cells have the type-0 phase mask, the input sound patterns can be exactly replicated at the free-space diffraction distance z as integer Talbot effect, if z is equal to even integer multiples of the Talbot distance $L = D^2/\lambda$ (D is the spatial period of the grating pattern and λ is the wavelength) [18]. At the diffraction distance $z = (m/n)L$ (m and n are any pair of mutually prime integers), the self-image of the original beam pattern can also be reproduced. But in such a case, not only the period of the self-image decreases by a factor of n along both x and y dimensions to become D' equal to D/n, but more importantly, the local beam density will change. It is the fractional Talbot effect [20,21]. For example, when $n$is set to be 2, the period would be divided by 2, as illustrated in Fig. 2(a).

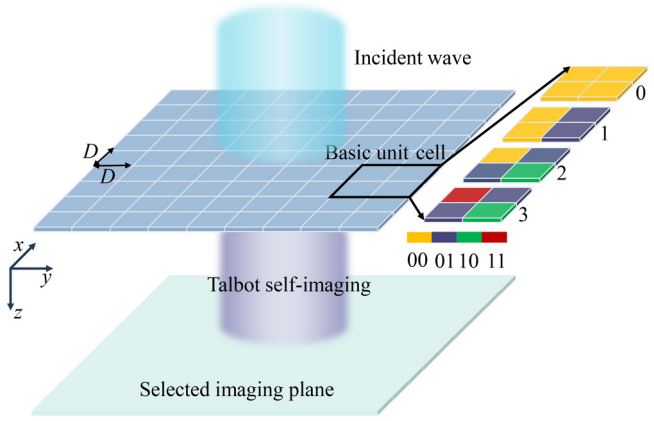

FIG. 1. An acoustic Talbot coding metasurface. An array of 2×2 elements forms a basic unit cell of the coding metasurface. Each element can provide one of the 0, $\pi/2$, π, and $3\pi/2$ phase-delay responses as one state in a 2-bit 4-digital states "00", "01", "10", and "11." With carefully designing each unit cell from four phase-mask candidates labeled as type 0–3, the Talbot coding metasurface can reproduce and amplify the incident sound patterns at the selected self-imaging plane.

Now considering sound propagation from plane $z = (m/n)L$ to $z' = (m'/n')L$ (where n and n' are coprime integers), a self-image of sound pattern at $z = (m/n)L$ with a period multiplied by a fractional factor n/n' can be recovered at z' [35]. If we would like to move the sound pattern at $z = (m/n)L$ to $z = 0$ as input, but keep the orginal self-image at $z' = (m'/n')L$ and the fractional factor n/n' intact, in this case, a phase mask must be added to z with additional phase modulation [35]:

$$\varphi_{i;a,b} = -\pi\frac{a}{b}i^2 - \pi c. \tag{1}$$

$i = 1, 2, 3, \ldots$ labels the element sequence number, a and b are coprime integers determined by m and n. c is a real constant that represents an equal phase shift for all the components. It has no effect on the performance of the self-image. Let E and O denote the sets of even and odd natural numbers, respectively. The expressions for a, b, and c as functions of m and n can be written as

$$m \in E, n \in O \; a = m\left[\left(\frac{1}{m}\right)_n\right]^2, b = n,$$
$$c = \frac{n+1}{4} - \frac{1}{2}\left(\frac{m}{n}\right), \tag{2}$$

$$m \in O, n \in O \; a = 8m\left[\frac{1}{2}\right]_n\left[\left(\frac{1}{2m}\right)_n\right]^2, b = n,$$
$$c = \frac{n+1}{4} - \frac{1}{2}\left(\frac{m}{n}\right), \tag{3}$$

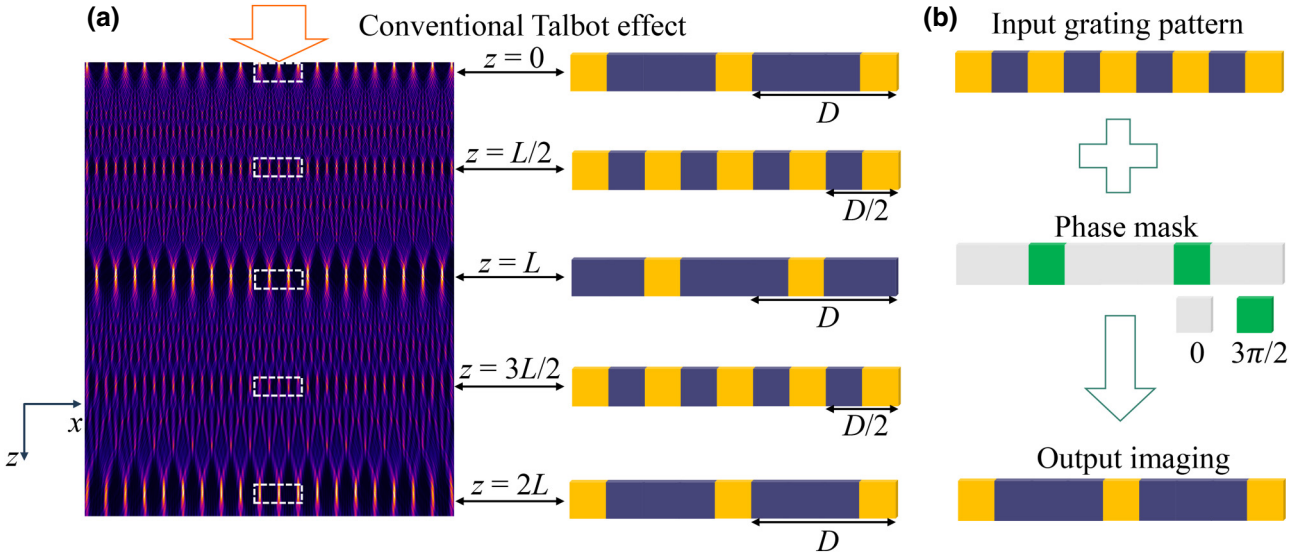

FIG. 2. (a) For conventional Talbot effect, the self-image period and intensity fall by a factor of 2 at the plane $z = L/2$ and $z = 3L/2$, while remaining unchanged at the integer multiples of Talbot length L. (b) When moving the sound-beam pattern at $z = L/2$ to $z = 0$ as the new input, adding a phase mask will keep the self-image at $z = 2L$ intact. The period and intensity is thus double that of the input. The gray and green units denote the required 0 and $3\pi/2$ phase modulation at each element.

$$m \in O, n \in E \; a = m\left[\left(\frac{1}{m}\right)_n\right]^2, b = n,$$
$$c = -\frac{n+2}{4} + \frac{1}{2}\left(\frac{m}{n}\right). \tag{4}$$

In the above expressions, $[1/m]_n$ indicates the modular multiplicative inverse of the integer m modulo n and $\left(\frac{m}{n}\right)$ is the Jacobi symbol. After neglecting the insignificant constant term πc in Eq. (1), the phase profile for the 1D self-image (the period is i) in the fractional Talbot plane $z = (m/n)L$ becomes

$$\varphi_{m,n}(i) = -\pi \frac{m}{n}\left[\left(\frac{1}{m}\right)_n\right]^2 i^2, \tag{5}$$

where the product $mn \in E$. When the product $mn \in O$, the phase is given by

$$\varphi_{m,n}(i) = -8\pi \frac{m}{n}\left[\frac{1}{2}\right]_n\left[\left(\frac{1}{2m}\right)_n\right]^2 i^2. \tag{6}$$

In our work, m and n are chosen to be 1 and 2, respectively. As demonstrated in Fig. 2(b), when the sound pattern at $z = L/2$ is moved to $z = 0$ as input, attaching a phase mask will be able to keep the orginal self-image at $z = 2L$ [21] and the fractional factor intact. The period of sound beams at according diffraction distance $z = 2L$ now doubles that at the input with much increased sound intensity, leading to the Talbot sound-beam amplification. Here the required phase mask needs two different types of phase modulation, 0 and $3\pi/2$, caculated based on Eq. (5).

For the two-dimensional Talbot sound amplification, the required phase-modulation profile for each individual element labeled by integers i_x and i_y along the x and y directions is the sum of the two corresponding individual phase terms:

$$\varphi(i_x, i_y) = \varphi_{m_x,n_x}(i_x) + \varphi_{m_y,n_y}(i_y). \tag{7}$$

Based on Eq. (7), if sound-beam amplification is only required along one dimension, $3\pi/2$ phase delay is required for certain elements at input. If amplifications along both dimentions are prefered, such phase delay may become π. As a π phase shift does not alter the nature of the self-image according to Eq. (1), a phase value of $\pi/2$ that corresponds to $3\pi/2$ can be introduced, so that the values 0, $\pi/2$, π, and $3\pi/2$ can act as the "00", "01", "10", and "11" elements in the 2-bit coding. By arranging the sequences of these four elements in the metasurface lens, self-imaging patterns and Talbot sound amplification can be flexibly tailored.

III. SIMULATED TALBOT AMPLIFICATION EFFECT

Numerical simulations are conducted with calculated phase profiles for coding metasurface composed of an array of 13 × 13 elements and placed at $z = 0$, to demonstrate the pattern-controllable self-imaging and sound-beam amplification effect. Each element is a square plate (the width $D = 6$ cm) embedded with a circular disk (the

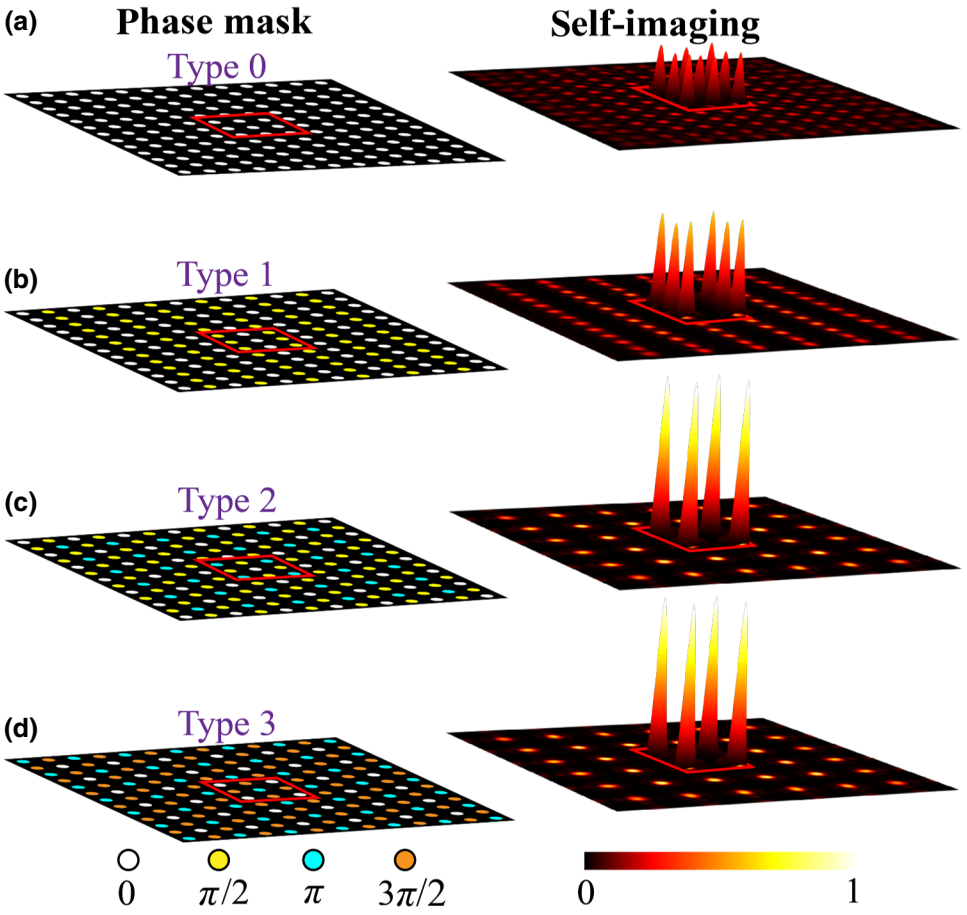

FIG. 3. Simulated Talbot sound amplification for different metasurfaces. Left column shows the metasurfaces at the input applied with different types of phase masks. Right column shows the sound beam applied, only the area inside the red square is shown. (a) Conventional Talbot effect (type 0), no phase modulation to the input. (b) Asymmetric Talbot effect with type-1 phase modulation (0 and $\pi/2$), only the spatial period along one direction is multiplied by 2. (c) Symmetric Talbot effect with type-2 phase modulation (0, $\pi/2$, and π), the spatial periods along two dimensions both are multiplied by 2. (d) Symmetric Talbot effect with type-3 phase modulation (0, π, and $3\pi/2$), the self-imaging pattern is the same as (c). For all the plots in (a)–(d), the left side is the phase mask applied in the input grating, the right side is the according self-image in the plane $z = 2L$ ($L = D^2/\lambda$). D is the spatial period of the input gratings along the two grating dimensions, and λ is the wavelength of the incident wave.

diameter $R = 4$ cm) at the center that provides effective phase response (for details see the Supplemental Material [36]). The basic unit cell of the phase mask is composed of 2×2 elements, tuned to have one of the four different phase responses that can resemble a 2-bit state as shown in Fig. 1. Periodic repeat of the unit cells will constitute the four different phase masks with various coding sequences.

How sound-field distribution on the self-imaging plane changes upon different phase modulations is simulated with COMSOL Multiphysics. The operating frequency is set at 10 kHz with a wavelength of 3.43 cm. As shown in Fig. 3, asymmetrical or symmetrical multiplication of self-imaging pattern periodicity can be realized by different encoded phase modulations. For conventional Talbot effect, the metasurface does not need any additional phase modulation. All elements are "'00." In this case, the incident wave pattern can be fully replicated at $z = 0.21$ m, as shown in the right subplot of Fig. 3(a). If two elements "00" and "01" are utilized to form phase-mask type 1, the corresponding phase modulation will double the spatial period D of sound pattern along one imaging plane direction, while the spatial period along the other direction remains unchanged [right column, Fig. 3(b)]. With three coding elements "00", "01", and "10", a type-2 phase mask can symmetrically multiplicate the spatial periods along both dimensions of the self-image by 2, as demonstrated in Fig. 3(c). The result of the type-3 phase mask with three elements "00", "10", and "11" is also presented in Fig. 3(d). The same imaging patterns in Figs. 3(c) and 3(d) demonstrate that a π phase shift will not alter the nature of the self-image, which verifies the theoretical prediction in Eq. (1).

The intriguing thing about this Talbot effect is it is almost lossless, with neglectable thermal and viscous losses in air. The intensity of each repeating individual pattern in the resulting self-image is thus multiplied by the product of the multiplication factors of periods along x and y directions. By comparing the sound-field distribution on the self-image plane after passing through four different phase masks, presented in the right column of Figs. 3(b)–3(d), the redistributed locally amplified sound field can be clearly observed. The corresponding energy-amplification factors for the cases in Figs. 3(b) and 3(c) are numerically calculated to be 2 and 4 (for details see the Supplemental Material [36]). By selecting different m and n, the required phase mask would

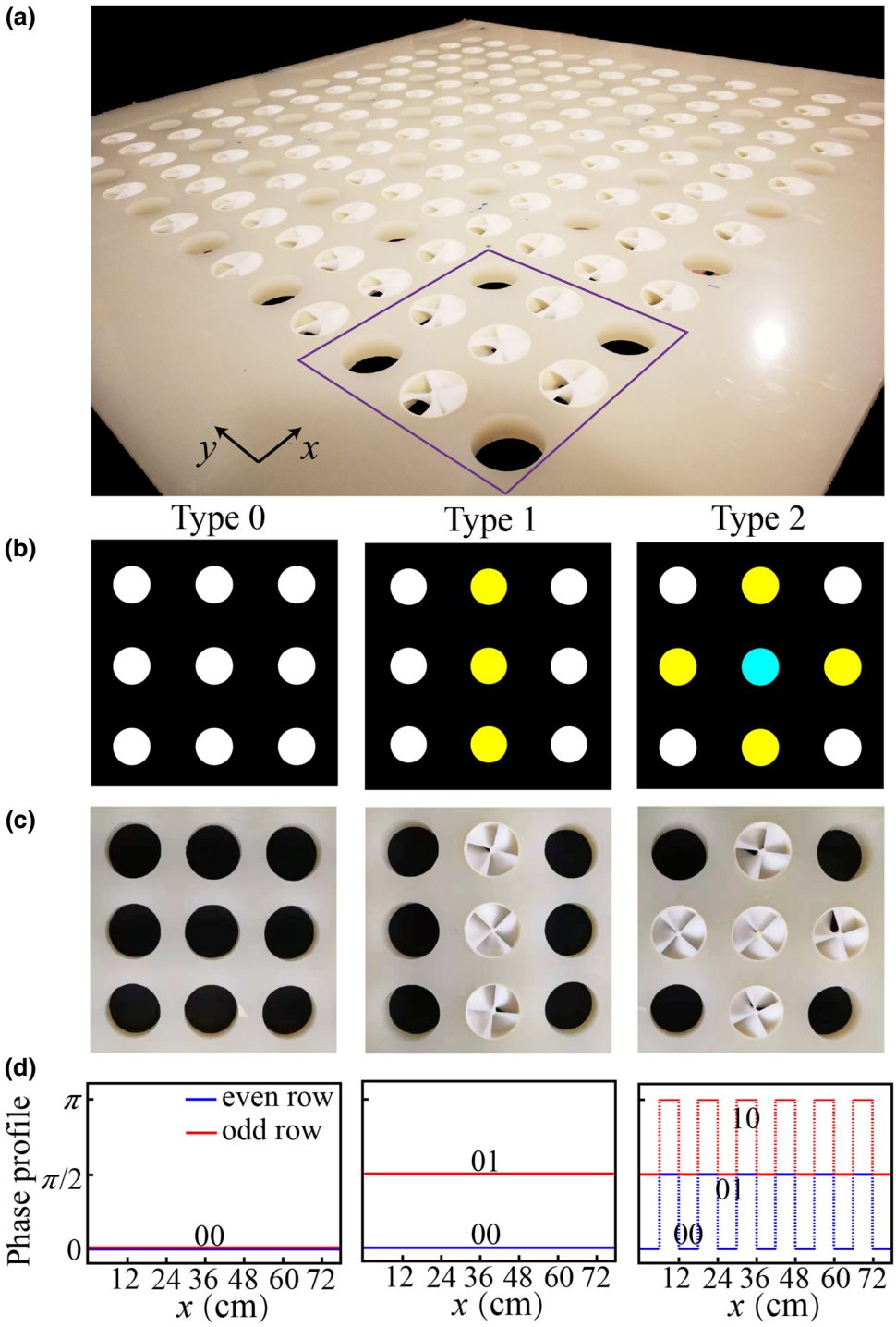

FIG. 4. (a) Fabricated sample with type-2 phase mask. (b) Schematics of phase-modulation arrangement within an area of 3 × 3 elements marked with a purple box in (a) for different phase masks. (c) Top view of the fabricated 3 × 3 element samples whose phase modulations are realized with different helical elements. (d) Phase profiles along the odd row (blue line) and even row (red line). "00", "01", and "10" represent the 0, $\pi/2$, and π phase modulation, respectively.

be different and the according amplification factor can be improved.

IV. DEMONSTRATION OF TALBOT SOUND AMPLIFICATION

Such passive amplification enabled by Talbot self-imaging as a result of the diffractive effect, tailors the local energy concentration to occur at some specific positions far away from any power source, offering the unique possibility of remote waveform enhancement. To experimentally demonstrate such a hypothesis, a coding metasurface lens with modular phase masks is fabricated, as shown in Fig. 4. Due to the nondispersive and low-loss nature, helicoid acoustic metamaterials [11,37–39] are employed to engineer the local phase-delay responses. The phase variation can be easily tuned by adjusting the thread lead of the helicoid units while keeping other geometric parameters unchanged (detail structures are presented in the Supplemental Material [36]). As the "00" element requires no phase modulation, only two groups of helicoid units are designed to, respectively, provide the $\pi/2$ and π phase delays. For the conventional Talbot effect, the top view of a perforated grating with no additional phase modulation of the 3×3 elements' region is presented in the left column of Fig. 4(c). By rearranging some elements with the "01" and "10" helicoid metamaterials, the coding lens with type-1 phase mask [middle column, Fig. 4(c)] and type-2 phase mask [right column, Fig. 4(c)] can be, respectively, constructed. The phase profiles along the odd and even rows in all three cases are plotted in Fig. 4(d), which clearly show the configuration of the three coding elements ("00", "01", and "10"). It is worth mentioning that, since the rearrangement of phase delays can be accomplished with the insertion and withdraw of helicoid units, different phase masks can be readily realized with only one metamaterial framework in a programmable modular way.

The fabricated coding metasurface has been put on test with different phase masks. The self-imaging sound patterns on the output imaging plane are experimentally measured (experimental details are given in the Supplemental Material [36]). Owing to the periodicity of imaging patterns, only the sound fields within an area of 3×3 units at the lens center are presented. As shown in Fig. 5, the overall measured sound-field distributions agree well with the simulation results. Without phase modulation, conventional Talbot effect guarantees that the incident wave pattern can be faithfully reproduced as presented in the numerical and experimental results. The measured sound field after adding a type-1 phase mask exhibits an asymmetric amplification, as demonstrated in Fig. 5(f). While the period along the x direction is doubled, the three peaks along the y direction are still intact. When the metasurface is coded with type-2 sequence, four, instead of the original nine, bright spots, arranged in a 2×2 way, appear on the self-imaging plane. The spatial periods along

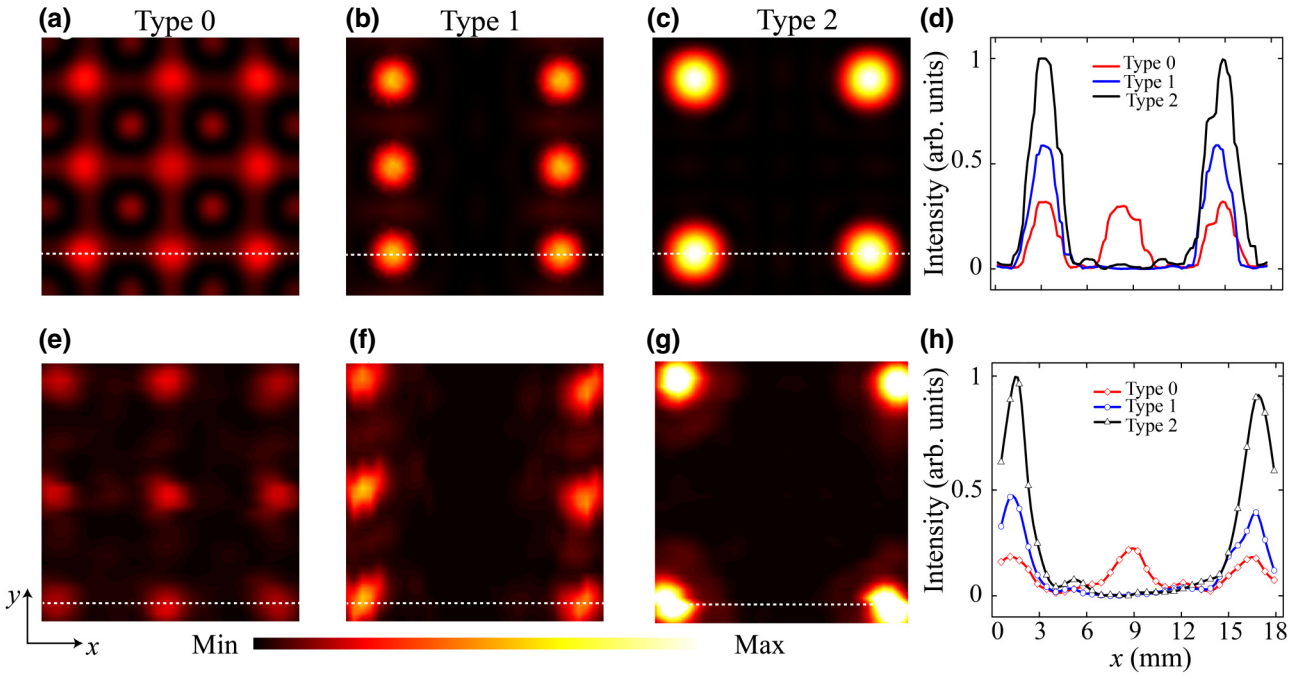

FIG. 5. Simulated and measured Talbot self-image patterns. (a)–(c) Simulated acoustic intensity distributions for an area of 3×3 elements (in the center of the metasurface) with type-0, type-1, and type2 phase masks. (d) Normalized acoustic intensity profiles along the white dashed lines in (a)–(c). (e)–(g) Measured acoustic fields corresponding to (a)–(c), respectively. (h) Normalized acoustic field distributions along the white dashed lines in (e)–(g).

both directions are obviously multiplied by 2, together with much amplified peak intensity. To further evaluate the sound concentration and local energy amplification, the normalized intensity profiles for all three metasurface phase-mask configurations, as marked by the white dashed lines, are presented in Figs. 5(h) and 5(d). The sound intensity increase of the bright spots from conventional Talbot effect to adding type 1 and type 2 phase modulations can be clearly observed. Moreover, this acoustic bidimensional Talbot effect is available over a certain bandwidth (refer to the Supplemental Material [36]), enabled by the broad working frequency range of the helicoid metamaterials.

V. CONCLUSIONS

In summary, we develop and experimentally examine a reconfigurable coding acoustic metasurface lens that can modulate the far-field sound-beam pattern and energy distribution. The combination of bidimensional Talbot self-imaging effect with flexible phase modulation can passively concentrate acoustic waves and produce local sound amplification at specific far-field locations. By conducting modularized arrangement of coding sequences, the sound-field distribution and amplification factor can be tuned. The spectral performance of the coding metasurface has also been experimentally confirmed. Our study suggests that bidimensional Talbot effect combined with phase modulation can act as an efficient approach to achieve far-field energy enhancement in free space. It offers a perspective to explore more functionalities of Talbot self-imaging in acoustics.

Furthermore, the produced amplification function shows great potential applications in particle manipulations, acoustic communications, imaging and signal processing. For instance, passive amplification of the repeating pattern in an input image may enable the extraction of this pattern from a noisy background, which is impossible with conventional gain-based image-amplification methods [40].

ACKNOWLEDGMENTS

The work is supported by the National Natural Science Foundation of China (Grant No. 11774297) and the General Research Fund of Hong Kong RGC (Grant No. PolyU 152119/18E).

[1] M. Xiao, G. Ma, Z. Yang, P. Sheng, Z. Zhang, and C. T. Chan, Geometric phase and band inversion in periodic acoustic systems, Nat. Phys. **11**, 3 (2015).

[2] K. Kim, C. I. Park, H. Lee, and Y. Kim, Near-zero effective impedance with finite phase velocity for sensing and actuation enhancement by resonator pairing, Nat. Commun. **9**, 1 (2018).

[3] M. Fatemi and J. F. Greenleaf, Ultrasound-stimulated vibro-acoustic spectrography, Science **280**, 5360 (1998).

[4] Y. Cheng, C. Zhou, B. Yuan, D. Wu, Q. Wei, and X. Liu, Ultra-sparse metasurface for high reflection of low-frequency sound based on artificial Mie resonances, Nat. Mater. **14**, 10 (2015).

[5] X. Zhu, B. Liang, W. Kan, Y. Peng, and J. Cheng, Deep-subwavelength-scale Directional Sensing Based on Highly Localized Dipolar Mie Resonances, Phys. Rev. Appl. **5**, 5 (2016).

[6] Y. Chen, H. Liu, M. Reilly, H. Bae, and M. Yu, Enhanced acoustic sensing through wave compression and pressure amplification in anisotropic metamaterials, Nat. Commun. **5**, 5247 (2014).

[7] J. Zhu, Y. Chen, X. Zhu, F. J. Garcia-Vidal, X. Yin, W. Zhang, and X. Zhang, Acoustic rainbow trapping, Sci. Rep. **3**, 1728 (2013).

[8] V. Romero-García, R. Picó, A. Cebrecos, V. J. Sánchez-Morcillo, and K. Staliunas, Enhancement of sound in chirped sonic crystals, Appl. Phys. Lett. **102**, 9 (2013).

[9] H. Jia, M. Lu, X. Ni, M. Bao, and X. Li, Spatial separation of spoof surface acoustic waves on the graded groove grating, J. Appl. Phys. **116**, 12 (2014).

[10] K. L. Tsakmakidis, O. Hess, R. W. Boyd, and X. Zhang, Ultraslow waves on the nanoscale, Science **358**, 6361 (2017).

[11] X. Zhu, K. Li, P. Zhang, J. Zhu, J. Zhang, C. Tian, and S. Liu, Implementation of dispersion-free slow acoustic wave propagation and phase engineering with helical-structured metamaterials, Nat. Commun. **7**, 11731 (2016).

[12] T. Liu, S. Liang, F. Chen, and J. Zhu, Inherent losses induced absorptive acoustic rainbow trapping with a gradient metasurface, J. Appl. Phys. **123**, 9 (2018).

[13] B.-I. Popa, Broadband sound pressure enhancement in passive metafluids, Phys. Rev. B **96**, 9 (2017).

[14] H.-S. Kwon and B.-I. Popa, Design and experimental demonstration of broadband acoustic pressure enhancing passive metafluids, J. Acoust. Soc. Am. **145**, 6 (2019).

[15] Y. Jin, X. Fang X, Y. Li, and D. Torrent, Engineered Diffraction Gratings for Acoustic Cloaking, Phys. Rev. Appl. **11**, 011004 (2019).

[16] Y. Jin, R. Kumar, O. Poncelet, O. Mondain-Monval, and T. Brunet, Flat acoustics with soft gradient-index metasurfaces, Nat. Commun. **10**, 1 (2019).

[17] H. F. Talbot, LXXVI. Facts relating to optical science. The London, Edinburgh, and Dublin Philosophical Magazine and Journal of Science **9**, 56 (1836).

[18] L. Rayleigh, XXV. On copying diffraction-gratings, and on some phenomena connected therewith. The London, Edinburgh, and Dublin Philosophical Magazine and Journal of Science **11**, 67 (1881).

[19] M. V. Berry and S. Klein, Integer, fractional and fractal Talbot effects, J. Mod. Opt. **43**, 10 (1996).

[20] L. R. Cortés, R. Maram, and J. Azaña, Fractional averaging of repetitive waveforms induced by self-imaging effects, Phys. Rev. A **92**, 4 (2015).

[21] H. G. de Chatellus, L. R. Cortés, A. Deville, M. Seghilani, and J. Azaña, Diffraction-induced Bidimensional Talbot Self-Imaging with Full Independent Period Control, Phys. Rev. Lett. **118**, 13 (2017).

[22] J. Jeon, R. Maram, J. van Howe, and J. Azaña, Programmable passive Talbot optical waveform amplifier, Opt. Express **26**, 6 (2018).

[23] R. Maram, J. Van Howe, M. Li, and J. Azana, Noiseless intensity amplification of repetitive signals by coherent addition using the temporal Talbot effect, Nat. Commun. **5**, 5163 (2014).
[24] C. Siegel, F. Loewenthal, and J. Balmer, A wavefront sensor based on the fractional Talbot effect, Opt. Commun. **194**, 4 (2001).
[25] A. Isoyan, F. Jiang, Y. Cheng, F. Cerrina, P. Wachulak, L. Urbanski, J. Rocca, C. Menoni, and M. Marconi, Talbot lithography: Self-imaging of complex structures, J. Vac. Sci. Technol. B **27**, 6 (2009).
[26] M. R. Dennis, N. I. Zheludev, and F. J. G. de Abajo, The plasmon Talbot effect, Opt. Express **15**, 15 (2007).
[27] H. F. Zhu and F. Semperlotti, Phononic thin plates with embedded acoustic black holes, Phys. Rev. B **91**, 10 (2015).
[28] D. Roshchupkin, L. Ortega, A. Snigirev, and I. Snigireva, X-ray imaging of the surface acoustic wave propagation in $La_3Ga_5SiO_{14}$ crystal, Appl. Phys. Lett. **103**, 15 (2013).
[29] H. Gao, Z. Gu, B. Liang, X. Zou, J. Yang, J. Yang, and J. Cheng, Acoustic focusing by symmetrical self-bending beams with phase modulations, Appl. Phys. Lett. **108**, 7 (2016).
[30] T. J. Cui, M. Q. Qi, X. Wan, J. Zhao, and Q. Cheng, Coding metamaterials, digital metamaterials and programmable metamaterials, Light Sci. Appl. **3**, 10 (2014).
[31] X. G. Zhang, W. X. Tang, W. X. Jiang, G. D. Bai, J. Tang, L. Bai, C. W. Qiu, and T. J. Cui, Light-controllable digital coding metasurfaces, Adv. Sci. **5**, 11 (2018).
[32] C. Della Giovampaola and N. Engheta, Digital metamaterials, Nat. Mater. **13**, 12 (2014).
[33] B. Xie, K. Tang, H. Cheng, Z. Liu, S. Chen, and J. Tian, Coding acoustic metasurfaces, Adv. Mater. **29**, 1603507 (2017).
[34] L. Zhang, X. Q. Chen, S. Liu, Q. Zhang, J. Zhao, J. Y. Dai, G. D. Bai, X. Wan, Q. Cheng, and G. Castaldi, Space-time-coding digital metasurfaces, Nat. Commun. **9**, 1 (2018).
[35] L. R. Cortés, H. G. de Chatellus, and J. Azaña, On the generality of the Talbot condition for inducing self-imaging effects on periodic objects, Opt. Lett. **41**, 2 (2016).
[36] See Supplemental Material at http://link.aps.org/supplemental/10.1103/PhysRevApplied.14.054067 for the four coding elements in the metasurface, intensity distributions for three coding sequences, printed helicoid structures, experimental setup and bidimensional Talbot effect over spectrum.
[37] S. Liang, T. Liu, F. Chen, and J. Zhu, Theoretical and experimental study of gradient-helicoid metamaterial, J. Sound Vib. **442**, 482 (2019).
[38] X. Zhu, K. Li, P. Zhang, J. Zhu, J. Zhang, C. Tian, and S. Liu, Implementation of dispersion-free slow acoustic wave propagation and phase engineering with helical-structured metamaterials, Nat. Commun. **7**, 1 (2016).
[39] S.-W. Fan, S.-D. Zhao, A.-L. Chen, Y.-F. Wang, B. Assouar, and Y. Wang, Tunable Broadband Reflective Acoustic Metasurface, Phys. Rev. Appl. **11**, 4 (2019).
[40] C. M. Caves, Quantum limits on noise in linear amplifiers, Phys. Rev. D **26**, 8 (1982).